

Modelling and numerical simulation of the in vivo mechanical response of the ascending aortic aneurysm in Marfan syndrome

Claudio M. García–Herrera¹ · Diego J. Celentano² · Emilio A. Herrera³

Received: 18 November 2015 / Accepted: 11 May 2016 / Published online: 1 June 2016
© International Federation for Medical and Biological Engineering 2016

Abstract Marfan syndrome (MFS) is a genetic disorder that affects connective tissue, impairing cardiovascular structures and function, such as heart valves and aorta. Thus, patients with Marfan disease have a higher risk of developing circulatory problems associated with mitral and aortic valves prolapse, manifested as dilated aorta and aortic aneurysm. However, little is known about the bio-mechanical characteristics of these structures affected with MFS. This study presents the modelling and simulation of the mechanical response of human ascending aortic aneurysms in MFS under in vivo conditions with intraluminal pressures within normotensive and hypertensive ranges. We obtained ascending aortic segments from five adults with MFS subjected to a vascular prosthesis implantation replacing an aortic aneurysm. We characterised the arterial samples via ex vivo tensile test measurements that enable fitting the material parameters of a hyperelastic isotropic constitutive model. Then, these material parameters were used in a numerical simulation of an ascending aortic aneurysm subjected to in vivo normotensive and hypertensive conditions. In addition, we assessed different constraints related to the movement of the aortic root. Overall, our results provide not only a realistic description of the mechanical behaviour

of the vessel, but also useful data about stress/stretch-based criteria to predict vascular rupture. This knowledge may be included in the clinical assessment to determine risk and indicate surgical intervention.

Keywords Human aorta · Marfan syndrome · Finite elements

1 Introduction

The Marfan syndrome (MFS) is a dominant autosomic genetic disorder that affects the elastic fibres of the connective tissue and is closely related to cardiovascular problems [25, 35]. For instance, MFS induces aortic dissections (layer separation of the artery) and/or thoracic aneurysms that present dilatations in the ascending region, usually in the vicinity of the aortic root [24]. As a consequence, the elastic response of the artery is severely jeopardized reducing both the strength of the aortic wall and its damping capacity of the intravascular pressure. This, in turn, impairs the conversion of the intermittent nature of the blood flow coming from the heart into a continuous flow [29]. Moreover, the fast aortic growth observed in MFS is closely related to a high risk of rupture and/or dissection at early ages (24.8 years old in average), leading to a dramatic reduction in life expectancy and eventual death [25]. This has motivated clinical and biomedical research to develop predictive models of the mechanical behaviour of aortic aneurysms.

The clinical estimates of rupture and dissection risks are currently based primarily on the maximum diameter and growth rate. However, these parameters cannot reflect the complex changes of the vessel wall morphology, and therefore, more data are needed to complement the information

✉ Claudio M. García–Herrera
claudio.garcia@usach.cl

¹ Departamento de Ingeniería Mecánica, Universidad de Santiago de Chile, USACH, Av. Bernardo O’Higgins 3363, Santiago de Chile, Chile

² Departamento de Ingeniería Mecánica y Metalúrgica, Instituto de Ingeniería Biológica y Médica, Pontificia Universidad Católica de Chile, Av. Vicuña Mackenna 4860, Santiago de Chile, Chile

³ Laboratorio de Función y Reactividad Vascular, ICBM, Facultad de Medicina, Universidad de Chile, Av. Salvador 486, Providencia Santiago de Chile, Chile

to decide an intervention [23]. The surgery to prevent rupture of the aneurysm has a significant risk, so it is only recommended when the risk of aneurysm rupture is higher than that of the surgery itself [11, 32]. In some cases, microscopic examination revealed an absence of the medial elastic fibres of not only the pathological wall but also in the vicinity of the aneurysm. This result justifies the entire aortic root replacement via the reimplantation technique, which has been found to be appropriate for the isolated aneurysm in one sinus of Valsalva in a patient affected by MFS [27].

Biomechanical *ex vivo* assessments, such as the uniaxial tensile, wire myograph, pressurisation (inflation–extension) and biaxial tests, have been extensively used to obtain relevant features of the pathological mechanical response and the conditions leading to material failure. Several indexes to estimate the aortic aneurysm elasticity and stiffness have also been defined in order to quantify the rupture stress and the wall strength along the different directions of the tissue [3, 10, 12, 13, 19, 30, 31, 33, 34, 36]. Furthermore, a slight anisotropic behaviour was observed in aneurysms in MFS [31]. However, an anisotropic response was found in some aneurysms not related to MFS, e.g. dilated ascending aortas [13, 15] and aneurysms caused by bicuspid aortic valve [15].

Several constitutive models that take into account the tissue morphology have been developed to phenomenologically describe the mechanical response of the aneurysm under physiological loads. Most of the studies using these models have been tested in abdominal aortic aneurysm (AAA) due to its higher prevalence and ease to obtain samples [8, 9, 22, 40, 42]. Numerical simulations based on a linear elastic isotropic law have been carried out to study the response of the aortic valve affected by the MFS when subjected to different aortic root dilatations response [18]. Furthermore, *in vivo* stress analysis of aortic arches under physiological conditions for healthy and MFS-related aneurysms using a linear elastic isotropic constitutive model to account for aortic root movements during the cardiac cycle has been reported [4, 5]. Aortic root movement and hypertension were found to significantly increase the longitudinal stress in the ascending aorta, demonstrating that the aortic insufficiency leads not only to an augmented stroke volume as a compensation mechanism, but also to increase the aortic root displacement in its axial direction. However, the physiological roles of neither the ligamentum arteriosum nor the aortic residual stresses were included in these studies. Since high anisotropy was not observed in arterial tissues affected by MFS, their mechanical response was described via an exponential isotropic strain energy function [26]. Analytical and numerical procedures to predict the the bulging mode of bifurcation and axial propagation in the context of aneurysm formation with cylindrical

geometry in cardiovascular diseases have been also explored [1, 2].

Clearly, there have been advances in the mechanical characterisation of the ascending thoracic aortic aneurysm (ATAA) in the last decade [35]. However, a comprehensive analysis including numerical modelling and experimental validation of the *in vivo* mechanical behaviour of an ATAA with the MFS is still a research subject to be explored.

We aimed in this work to biomechanically characterise and numerically simulate the *in vivo* behaviour of the human ascending aortic aneurysm in the MFS. The material and methods considered in this study, which encompass experimental procedures, modelling and material characterisation applied to a group of adult arteries with similar ages, are presented in Sect. 2 (Material and methods). The assessed aneurysms were firstly characterised via *ex vivo* uniaxial tensile test measurements that enable to fit by a least-squares procedure the material parameters of a non-linear hyperelastic isotropic constitutive model. It should be noted that the MFS aneurysms analysed exhibit a slight degree of anisotropy. Using these material parameters, Sect. 3 (Results) presents the results of the tensile response and the numerical modelling of ascending aortas with Marfan aneurysms subjected to *in vivo* conditions with normotensive and hypertensive pressure levels. In addition, the experiment was performed under different conditions related to the movement of the aortic root. Relevant aspects related to the geometry, boundary conditions and initial stresses considered in the analysis are specifically detailed in this section. Finally, our findings discussed in Sect. 4 were found to provide a realistic description of the biomechanical responses of the aneurysm. These predictions together with an adequate definition of stress/stretch-based criteria may allow an appropriate diagnosis of the risk of failure at damaged zones of the aneurysm.

2 Material and methods

2.1 Ascending aorta samples

The MFS aortas came from five adult patients with MFS who were subjected to vascular prosthesis implantation surgery (Table 1). A representative picture of these dilated aortas is shown in Fig. 1. The pathological condition of the tissue was confirmed by a histological analysis. Briefly, small pieces of tissue were extracted from each artery along its longitudinal and circumferential directions (parallel and perpendicular to the vessel axis, respectively). Each segment of tissue was fixed in formaldehyde 4 %, embedded in paraffine and subsequently treated with hematoxyline–eosine to observe nuclei and elastin–collagen packages. In addition, van Gieson staining was used to identify elastin

Table 1 Data of patients with Marfan aneurysm in the ascending aorta

Vessel	Sex	Age (years)	Weight (kg)	Height (m)
1	F	58	71	1.66
2	M	69	88	1.70
3	M	55	86	1.80
4	M	50	76	1.76
5	F	57	73	1.69

and collagen fibres. Images of the vessels were taken in order to quantify nuclei, elastin and collagen plus the distribution of elastin and collagen fibres.

2.2 Constitutive modelling

According to the measurements reported in Sect. 3.1, an elastic, isotropic and rate-independent material response is considered for the arteries analysed in the present work. Moreover, their behaviours are taken as incompressible due to the large amount of water present in them. To this end, hyperelastic constitutive models can be used to describe their mechanical response. In this context, a deformation energy function W , assumed to describe the isothermal material behaviour under any loading conditions, is usually defined in terms of the right Cauchy deformation tensor $C = F^T \cdot F$, where F is the deformation gradient tensor and T is the transpose symbol (note that $\det F = 1$ in this case). Invoking classical arguments of continuum mechanics, the Cauchy stress tensor σ is defined as $\sigma = 2F \cdot \frac{\partial W}{\partial C} \cdot F^T$. In particular, the energy function proposed by Demiray in [6] is expressed as:

$$W = \frac{a}{b} \left[\exp \left(\frac{b}{2} (I_1 - 3) \right) - 1 \right] \tag{1}$$

where I_1 is the first invariant of C ($I_1 = \text{tr}(C)$, tr being the trace symbol).

As shown in Sect. 3, this constitutive model is adopted in this work to assess its capabilities in the prediction of the mechanical behaviour of human aortic arch including the aneurysm with the MFS and the unaffected tissue. Although the Demiray model is used in the present study to assess the risk of rupture, it should be noted that it cannot predict the risk of dissection since it does not take into account the layered nature of the tissue.

2.3 Biomaterial characterisation via the uniaxial tensile test

Ex vivo uniaxial tensile tests were carried out in order to determine the biomechanical behaviour of the aortic samples. The samples were cut along the longitudinal, diagonal and circumferential directions in order to characterise the degree of anisotropy in the material response. They were extracted from the anterior and posterior regions of the ascending aorta. All tests were performed immediately after dissection and after a maximum period of 24 h (i.e. 1 day from the time of replacement to testing). The tests were carried out with the specimens submerged in physiological serum (PBS) at a temperature of $37 \pm 0.5^\circ \text{C}$. In order to achieve uniform conditions for each sample, a time interval of 10 min was considered between the end of the assembly and the beginning of the test. To precondition the samples, ten successive loading cycles were executed up to a stress value of around 10 % of the rupture threshold (100 and 300 kPa for the aneurysmal and unaffected zones of the aorta, respectively). Axial load and axial jaws displacement were recorded during the whole test (the frequency of data acquisition was 10 measurements per second). The uniformity of the strain field was checked with an optical strain measurement

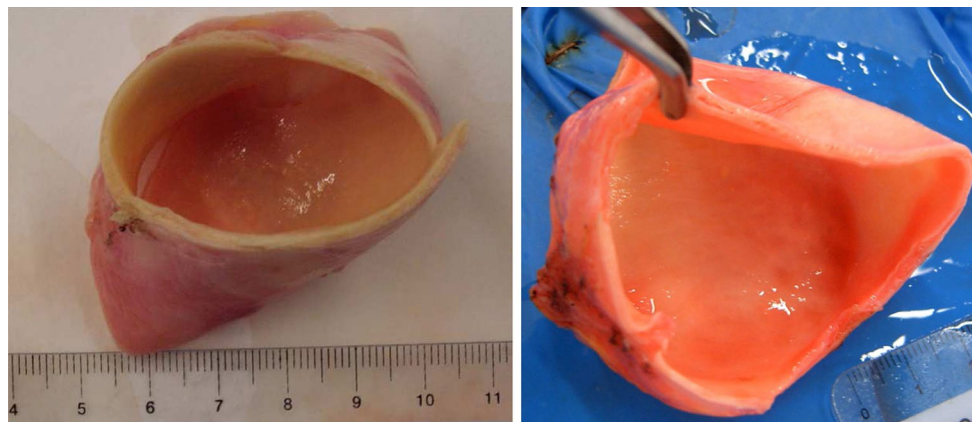


Fig. 1 Representative segments of dilated ascending aortas with Marfan syndrome

device. Further details of the experimental procedure are described elsewhere [16].

The uniaxial tensile test measurements reported in Sect. 3.1 are used in this study to determine the biomaterial parameters of the exponential constitutive law presented above. The true axial stress associated with the loading direction 1 was computed as $\sigma_1 = F/A$, where F is the axial load and A is current transversal area of the sample. For this model, this stress can be exclusively written in terms of the related axial stretch $\lambda_1 = L/L_0$, with L and L_0 being the current and initial sample lengths, respectively. This relationship is:

$$\sigma_1 = a \left(\lambda_1^2 - \frac{1}{\lambda_1} \right) \exp \left[\frac{b}{2} \left(\lambda_1^2 + \frac{2}{\lambda_1} - 3 \right) \right] \quad (2)$$

In this case, a linear least-squares fitting procedure to obtain the biomaterial parameters a and b was achieved [16]. The resulting biomaterial parameters for both the unaffected and MFS tissues are presented in Sect. 3.1.

Data processing and statistics: at least 12 specimens were tensile-tested for each aneurysm, four in each of the three directions (longitudinal, diagonal and circumferential). The same procedure was performed for the unaffected part of the vessel. All in all, 145 tests on ascending aortic tissue were carried out. The value of the rupture stress defined above was averaged for each group and orientation (only longitudinal and circumferential due to the nearly isotropic character of the tissue). Data are presented as mean \pm SD. An unpaired 2-tailed Student's t test was performed to compare the rupture stress. Significance was assumed for p as less than 0.05.

3 Results

All patients were adults between 50 and 69 years old; see Table 1. The experimentally measured maximum diameter and thickness values at the aneurysmal zone of the ascending aorta were 47.5 ± 2.5 mm and 2.0 ± 0.15 mm, respectively consistent with previous reports [31].

3.1 Uniaxial test

The average experimental stress–stretch curves obtained up to the rupture stage along the circumferential and longitudinal directions for the aneurysmal zone are plotted in Fig. 2a, evidencing good repeatability between measurements. Furthermore, the stress–stretch curves along the diagonal direction (i.e. 45° with respect to the axial direction) showed no significant differences with those along the circumferential and longitudinal directions over the whole stretch range up to rupture [(1.0–1.65), data not shown]. Thus, the biomechanical response can be assumed as practically isotropic,

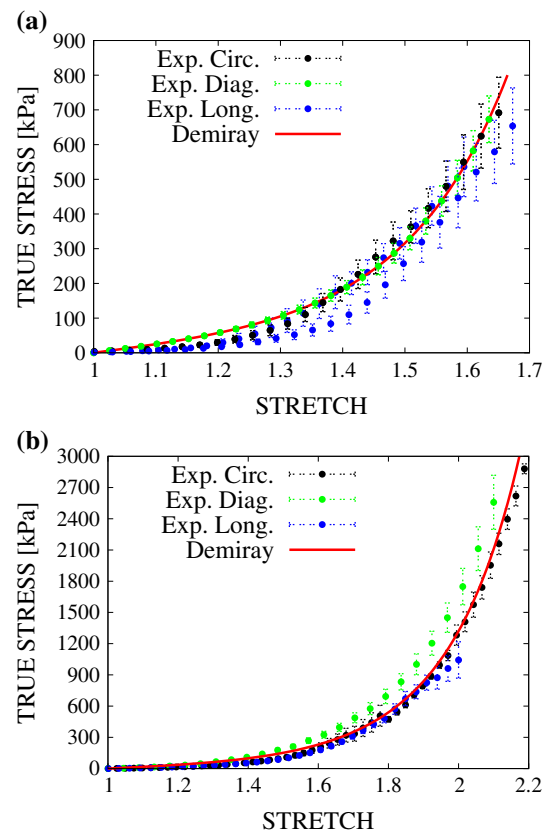


Fig. 2 Experimental data and computed results of true stress versus stretch along the circumferential, diagonal and longitudinal directions for **a** the aneurysmal zone ($a = 79.613$ kPa and $b = 3.152$; $r^2 = 0.989$) and **b** the unaffected part of the aortic arch ($a = 54.419$ kPa and $b = 1.936$; $r^2 = 0.996$)

since its stiffness is mainly provided by the elastin component of the tissue. In addition, the rupture stress values corresponding to both directions are similar. Moreover, it should be noted that similar biomaterial behaviours were observed at different positions around the circumference and along the length of the aneurysm. Therefore, these two aspects (i.e. material isotropy and homogeneity) justify that an adequate description of the biomaterial response can be simply tackled by means of the constitutive law expressed by Eq. 2. This argument is valid for both the affected and unaffected parts of the aortic arch until a stretch value of 1.7.

The stress–stretch curves obtained by applying a least-squares fitting of Eq. 2 to the corresponding experimental data are also plotted in Fig. 2a. In addition, the tensile response of the unaffected portion of the arch was characterised by the same methodology described above. In this case, the average experimental stress–stretch curves along the circumferential and longitudinal directions are plotted in Fig. 2b.

The resulting two sets of material parameters are used in the numerical simulation presented in Sect. 3.2.

3.2 Numerical simulation of an ascending aorta with a Marfan aneurysm

This section presents the numerical modelling of the bio-mechanical behaviour of the human aortic arch characterised in Sect. 3.1 under in vivo normotensive and hypertensive conditions (systolic pressures of 120 and 160 mmHg, respectively). Relevant analyses were performed and presented below.

3.2.1 Geometry and boundary conditions

The 3D simplified geometry of the human aortic arch used in the numerical simulation for this study was obtained from digital images of the samples considered in Sect. 2.1 complemented with anatomical dimensional data of adult aortas [4, 5, 38]. Figure 3 depicts the geometry considered in the present analysis.

The numerical simulation of this problem was carried out using the nonlinear constitutive model, and the corresponding material parameters, respectively, are presented in Sects. 2.3 and 3.1. This constitutive model has been implemented in an in-house finite element code extensively validated in many biomechanical applications [16, 17]. Moreover, the finite element mesh used in the simulations was composed of nearly 55,500 nodes and 44,000 isoparametric hexahedra. Four elements were considered along the wall thickness (assumed constant in the computations) in order to properly capture the stress radial gradients that may develop in the different regions of the aortic arch. It should be noted that this mesh is the result of a previous convergence study of the numerical response to different discretisations.

In vivo measurements on healthy and pathological patients during their cardiac cycle reported by [4, 5] are adopted here in order to define appropriate boundary conditions. They encompass three types of kinematic constraints. Firstly, the axial motion of the aortic root, caused by its connection to the left ventricle, consisting of an axial displacement of $u = 8.9$ mm and a rotation of $\phi_0 = 6^\circ$ (Fig. 3). Secondly, the other four edges of the aortic arch are assumed to be axially fixed and unconstrained along the radial direction. Thirdly, the effect of the ligamentum arteriosum is taken into account by means of a spring element with a stiffness ten times higher than that of the aortic arch tissue. Moreover, the presence of initial stresses was also taken into account with the procedure described in [17]. It is seen that the MFS damaged part of the tissue is only circumscribed to the aneurysm of the arch which is located in the ascending aorta. The elastic properties of the material in this pathological zone are clearly different from those of the unaffected tissue of the arch. In the numerical simulation, a linear transition between these two sets of

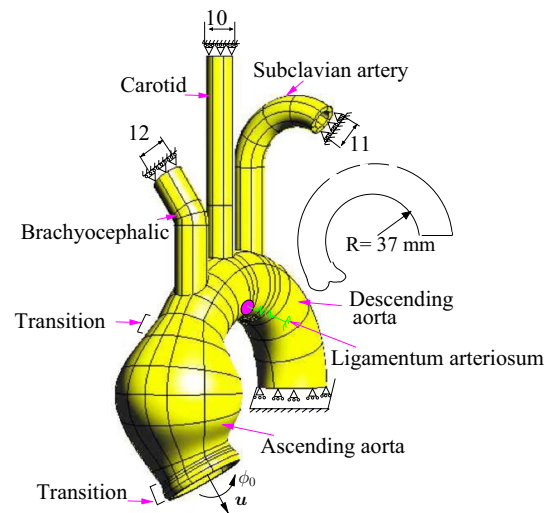


Fig. 3 Geometry and boundary conditions of the human ascending aorta considered in the analysis (dimensions in mm)

Table 2 Aortic segments studied

Case	P (mmHg)	u (mm)	ϕ_0 ($^\circ$)
ATAA1	120	4.3	0
	120	4.3	6
	160	4.3	6
ATAA2	120	8.9	0
	120	8.9	6
	160	8.9	6
ATAA3	120	15.0	6
	160	15.0	6

ATAA ascending thoracic aortic aneurysm

material properties was considered. Nevertheless, it should be noted that the present analysis is focused on the material’s response in the MFS region.

3.2.2 Stress fields

This study also aimed to compare the effect of the imposed boundary conditions on the mechanical response of the pathological ascending aorta. The cases shown in Table 2 are classified according to three values of the aortic root displacement u , since the rotation ϕ_0 was found by [4] to not strongly affect the vessel’s behaviour when a linear elastic isotropic model was used. Only the maximum values of pressure, aortic root displacement and rotation were considered in the analysis. The sections (INI: initial part, ANEU: aneurysm, ASC: ascending portion and UST: sinotubular joint) and regions (AN: front, RS: right, LS: left and PO: back) of the aneurysm considered for the analysis are shown in Fig. 4.

Table 3 Comparative analysis of the maximum principal stress in region AN and section ASC

Case	P (mmHg)	u (mm)	ϕ_0 (°)	σ_1 (kPa)
Healthy [4]	120	4.3	0	300
Healthy [4]	120	8.9	0	340
Healthy [4]	120	8.9	6	350
Aneurysmal root [5]	120	4.3	0	330
Healthy [17]	120	8.9	6	143
Healthy [17]	160	8.9	6	290
ATAA1	120	4.3	0	329
ATAA1	120	4.3	6	333
ATAA2	120	8.9	0	333
ATAA2	120	8.9	6	337
ATAA3	120	15	6	341
ATAA1	160	4.3	6	510
ATAA2	160	8.9	6	512
ATAA3	160	15	6	512

A comparative analysis of the maximum principal stress, including results of the literature and those of the MFS cases studied in the present work (i.e. ATAA1, ATAA2 and ATAA3), is summarised in Table 3.

The maximum principal stress contours at the deformed aneurysmal zone under normotensive (both diastolic and systolic) and hypertensive conditions for the ATAA2 case are plotted in Fig. 5. Different regions and sections are particularly analysed, showing the most critical zone for each loading condition.

Some clinical parameters of the analysed aneurysmal sections for the ATAA2 case are shown in Table 4. The pressure P and external diameter D of the ATAA in the diastolic and systolic conditions (subscripts d and s , respectively) allow the estimation of the vessel stretching capacity and stiffness. These features are usually quantified by means of the distensibility DC and the incremental modulus E_{inc} [21]:

$$DC = \frac{D_s^2 - D_d^2}{D_s^2(P_s - P_d)} \quad (3)$$

$$E_{inc} = \frac{3}{DC} \left(1 + \frac{D_d^2}{D_s^2 - D_{di}^2}\right) \quad (4)$$

where D_{di} is the internal diastolic diameter.

Finally, a comparative analysis of circumferential and longitudinal rupture stresses for the ATAA2 case is presented in Fig. 6, summarising the data of Figs. 2 and 5. The maximum values of σ_1 and σ_2 occur at the same AN region (see Fig. 5). Moreover, these stresses are effectively aligned with the circumferential and longitudinal directions in the critical locations. No distinction has been made between male and female specimens, as no significant differences between the two sexes have been found in the all experiments. Only directional differences in mechanical behaviour were found for unaffected specimens, where the circumferential failure stresses were greater than the longitudinal ones (2829 ± 112 vs. 1120 ± 101 kPa, $p = 0.001$).

4 Discussion

As shown in Fig. 2a, the MFS samples showed a nearly isotropic response. This behaviour has also been observed in MFS [31] and other types of aneurysms [33, 36, 37, 42]. In the present study, we showed that the MFS markedly affects the strength of the tissue in the stress–stretch ranges as depicted in Fig. 2a. These stress–stretch levels are different from those corresponding to the unaffected tissue (Fig. 2b).

The maximum principal stress values have been proposed as a risk index to predict the failure of aneurysmal tissues [7, 22, 41]. In agreement with the results that [4] computed with a linear elastic isotropic model, Table 3

Fig. 4 Schematic representation of the sections and regions considered for the analysis (sections *INI* initial part, *ANEU* aneurysm, *ASC* ascending portion, *UST* sinotubular joint; regions *AN* front, *RS* right, *LS* left, *PO* back)

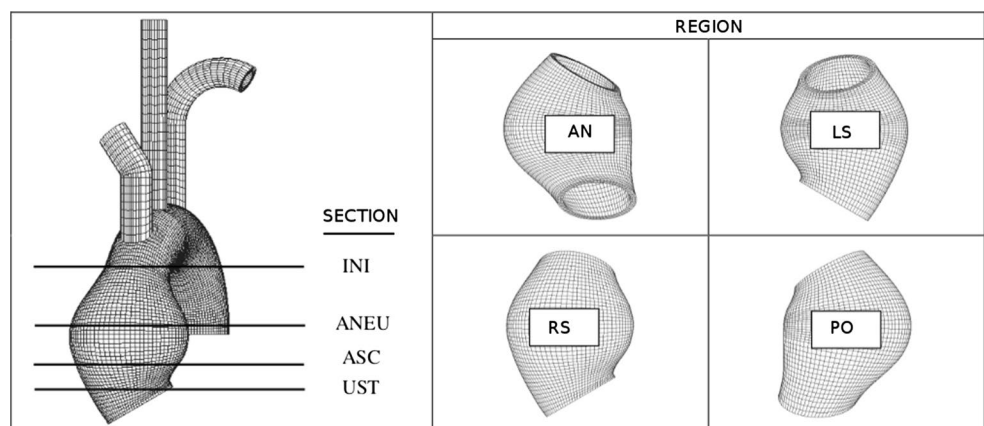


Fig. 5 Maximum principal stress (Pa) in the deformed aneurysmal zone under normotensive (diastolic and systolic) and hypertensive conditions for the ATAA2 case with $\phi_0 = 6^\circ$

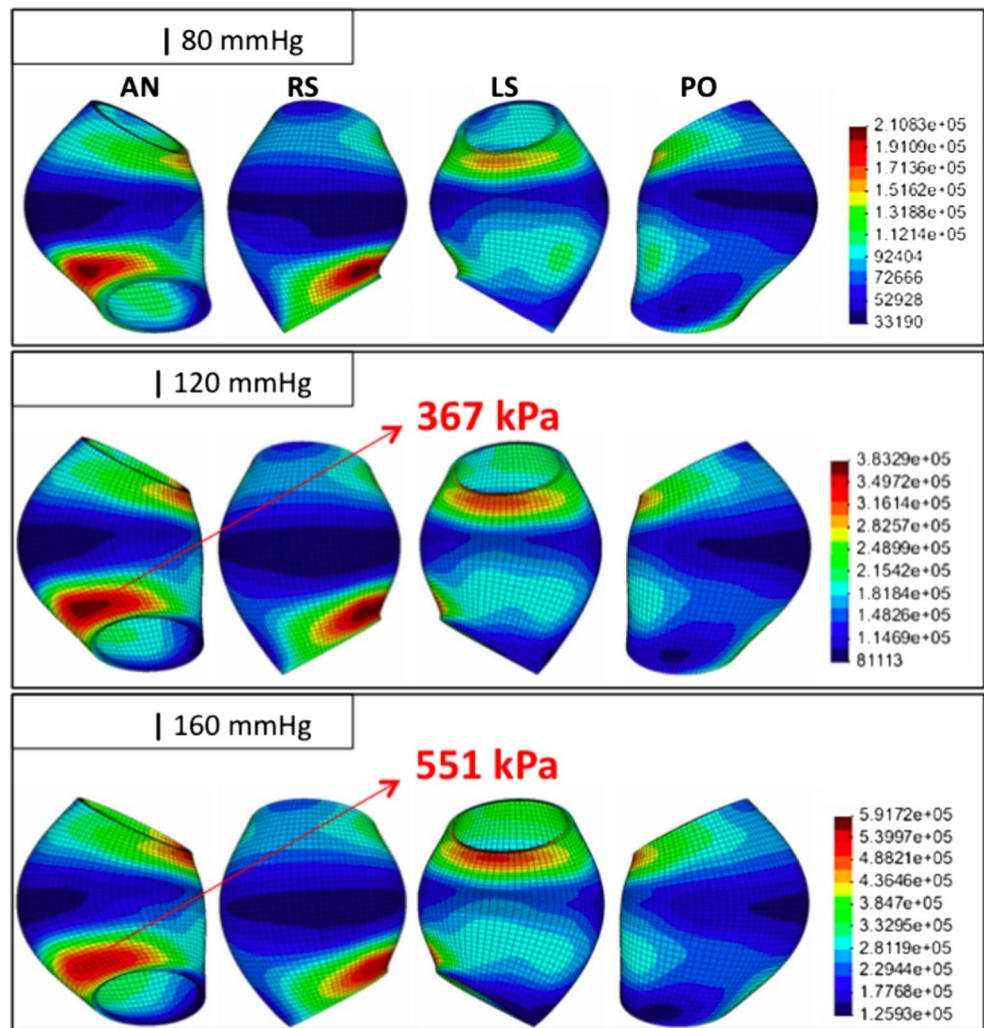


Table 4 Clinical parameters of the analysed aneurysmal sections for the ATAA2 case

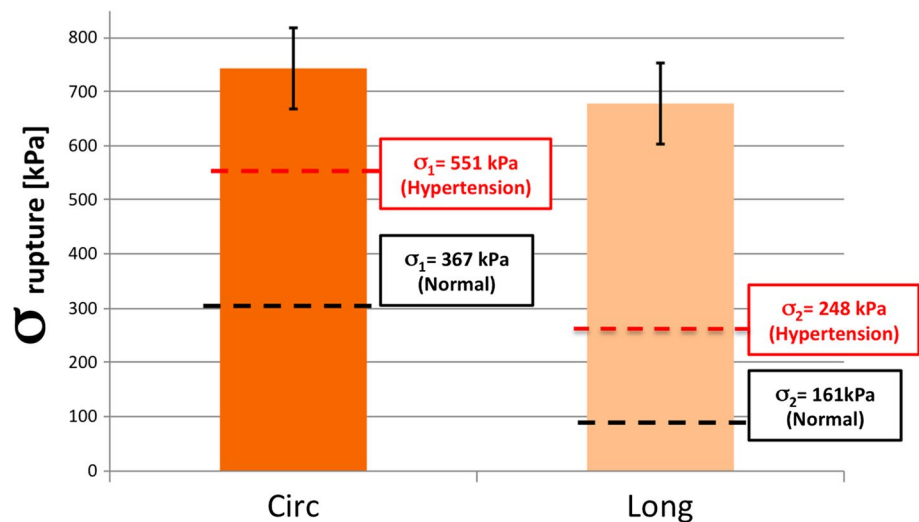
Section	$DC10^{-3}$ (mmHg^{-1})	E_{inc} (kPa)
INI	11.28	120
ANEU	7.92	291
ASC	10.72	163
UST	8.26	186

shows that the aortic root rotation was also found to not largely affect the vessel’s behaviour when the nonlinear hyperelastic isotropic model considered in the present analysis was used. In healthy tissues, it is seen that both constitutive models provide very different responses for the same loading conditions, i.e. the stress value for the linear law is nearly twice as that given by the hyperelastic law. Moreover, the stress results for the MFS cases studied in this work clearly show that the root displacement value does not play

a relevant role in the aneurysm’s response. For normotensive conditions, the stress levels corresponding to healthy tissues are similar to those of MFS aneurysms, regardless of the root displacement value. However, it should be noted that the risk of failure is greater in the latter, as very different stretch levels occur in these two types of tissues for the same stress value (Fig. 2). On the other hand, for hypertensive conditions, the effects of the MFS are evident since the two types of tissues experience very different stress levels (i.e. the stress value for the MFS tissue is approximately twice that of the healthy tissue) such that the stress value of the MFS case dangerously approaches its rupture stress (Fig. 2a).

Furthermore, the most clinically relevant ATAA2 case (Fig. 5) showed that although the stress distribution along the aortic wall does not significantly change with pressure variation, the maximum values are, as expected, highly influenced by the physiological loading. The critical points (i.e. maximum stress values) are located in either the distal or inflection zones which do not correspond to the region

Fig. 6 Comparative analysis of circumferential and longitudinal rupture stresses (kPa) under normotensive (systolic) and hypertensive conditions for the ATAA2 case with $\phi_0 = 6^\circ$; the bars correspond to the experimental average tensile rupture stress



where the aneurysm presents its maximum diameter. For normotensive conditions, the critical stresses in the upper inflection zone are located in region LS with maximum values of 296 and 171 kPa for the INI and ANEU sections, respectively. In general, lower stresses occur in section ANEU, which is the part of the vessel that presents the maximum dilatation. In the lower inflection zone, sections ASC and UST of region AN exhibit the maximum stress values, 367 and 268 kPa, respectively. This stress field has a mainly circumferential orientation with a nearly uniform distribution along the thickness of the aneurysm. For hypertensive conditions, the maximum stress values in the upper inflection zone are 495 and 293 kPa, which correspond to sections INI and ANEU, respectively. In the lower inflection zone, the maximum stress values located in sections AST and UST of region AN are 551 and 398 kPa, respectively. Once again, a negligible stress variation along the thickness was found in this case. In accordance with the results reported by [23, 28], the present numerical predictions also ratify that section ASC of region AN is the most critical zone prone to failure. However, the stress values shown in Fig. 5 are lower than those computed by [28] (i.e. the von Mises stress of section ASC of region AN are 350 and 400 kPa, respectively) since the latter were obtained via a linear elastic model with material parameters corresponding to a healthy tissue.

The computed values for the average thickness and maximum external diameter for the ascending aorta under the systolic pressure were 1.76 and 50.5 mm, respectively. These values were used to obtain the parameters listed in Table 4. It is seen that section ASC is more distensible than section ANEU, presumably due to the greater amount of damage in the former section. Similarly, the slightly greater distensibility of section ASC with respect to section UST is mainly associated with the higher stiffness of the latter section. The ANEU section shows, however, an enhanced

distensibility with a lower stiffness compared to a healthy tissue [14]. In general, the damage in pathological arteries leads to decreased elasticity of the tissue reflected in higher E_{inc} and lower DC values with respect to those of healthy tissues [20]. Nevertheless, the MFS causes an inverse effect, resulting in a more flexible passive mechanical response in terms of E_{inc} and DC [14, 20]. The mechanical behaviour computed in the present work for the ATAA is globally consistent with previous results [14, 20, 30, 39].

Figure 6 shows that the stress levels in the aneurysm for the ATAA2 case are close to rupture values measured in the tensile tests, mainly along the circumferential direction for the hypertensive condition (Fig. 2). Thus, the tissue of the aneurysm acts in the last part of the stress–stretch curve, where it presents the greatest stiffness, thereby reducing the damping capacity of the ascending aorta. These rupture stress values are lower than those of bicuspid aortic valve (BAV) patients [15]. Although these results are partially in agreement with previous data reported elsewhere [31], in which a significant difference between circumferential and longitudinal specimens of aneurysms in MFS was not found, the trend noted in Figs. 2 and 6 suggests that a small anisotropy could be present in both diseased and healthy aortic walls, as it has also been reported [19].

5 Conclusions

Experimental, modelling and simulation focused on the in vivo biomechanical behaviour of adult ATAAs with MFS have been presented. The pathologic tissue was firstly characterised via ex vivo tensile testing in order to obtain the rupture stress and stretch levels as well as the material parameters of a hyperelastic isotropic model adopted here. Thus, we properly described the aortic passive response

under normotensive and hypertensive conditions. This mechanical behaviour is found to be realistic, since the computed predictions are based on accurate experimental tensile test measurements that are scarce in the literature. The numerical simulations allowed the determination of the potential risky zones of the aneurysm quantified in terms of stress levels, distensibility and incremental modulus. It is concluded that the rupture stress for a MFS aneurysm exhibits lower values than those corresponding to BAV tissues. This fact is associated with the microstructure degeneration of the aneurysmal wall.

Several aspects must be addressed in future research in this area to translate this knowledge to the clinical practice, such as consideration of patient-specific geometry and more realistic boundary conditions aimed at achieving a better estimation of the stress pattern in the artery. Besides, more experimental approaches considering assessment of multi-layer constitutive models including the active behaviour and simulation of the influence of the blood flow on the biomechanical response of the aortic aneurysm with the MFS must be developed for a complete and effective prediction of the tissue behaviour.

Acknowledgments The supports provided by DICYT Project 051415GH of the Universidad de Santiago de Chile (USACH) and FONDECYT Grant No. 1151119 of the Chilean Council for Research and Technology (CONICYT) are gratefully acknowledged.

Compliance with ethical standards

Conflict of interest The authors declare no conflicts of interest.

References

- Alhayani AA, Giraldo JA, Rodriguez J, Merodio J (2013) Computational modelling of bulging of inflated cylindrical shells applicable to aneurysm formation and propagation in arterial wall tissue. *Finite Elem Anal Des* 73:20–29
- Alhayani AA, Rodriguez J, Merodio J (2014) Competition between radial expansion and axial propagation in bulging of inflated cylinders with application to aneurysms propagation in arterial wall tissue. *Int J Eng Sci* 85:74–89
- Azadani AN, Chitsaz S, Mannion A, Mookhoek A, Wisneski A, Guccione JM, Hope MD, Ge L, Tseng EE (2013) Biomechanical properties of human ascending thoracic aortic aneurysms. *Ann Thorac Surg* 96:50–58
- Beller CJ, Labrosse MR, Thubrikar MJ, Robicsek F (2004) Role of aortic root motion in the pathogenesis of aortic dissection. *Circulation* 109:763–769
- Beller CJ, Labrosse MR, Thubrikar MJ, Szabo G, Robicsek F, Hagl S (2005) Increased aortic wall stress in aortic insufficiency: clinical data and computer model. *Eur J Cardio-thorac Surg* 27:270–275
- Demiray H (1972) On the elasticity of soft biological tissues. *J Biomech* 5:309–311
- Di Martino ES, Vorp DA (2003) Effect of variation in intraluminal thrombus constitutive properties on abdominal aortic aneurysm wall stress. *Ann Biomed Eng* 31:804–809
- Doyle BJ, Cloonan AJ, Walsh MT, Vorp DA, McGloughlin TM (2010) Identification of rupture locations in patient-specific abdominal aortic aneurysms using experimental and computational techniques. *J Biomech* 43:1408–1416
- Doyle BJ, Killion J, Callanan A (2012) Use of the photoelastic method and finite element analysis in the assessment of wall strain in abdominal aortic aneurysm models. *J Biomech* 45:1759–1768
- Duprey A, Khanafer K, Schlicht M, Avril S, Williams D, Berger R (2010) In vitro characterization of physiological and maximum elastic modulus of ascending thoracic aortic aneurysms using uniaxial tensile testing. *Eur J Vasc Endovasc Surg* 39:700–707
- Erbel R, Eggebrecht H (2006) Aortic dimensions and the risk of dissection. *Heart* 92:137–142
- Ergin MA, Spielvogel D, Apaydin A, Lansman SL, McCullough JN, Galla JD, Griep RD (1999) Surgical treatment of the dilated ascending aorta: when and how? *Ann Thorac Surg* 67:1834–1839
- Ferrara A, Morganti S, Totaro P, Mazzola A, Auricchio F (2016) Human dilated ascending aorta: mechanical characterization via uniaxial tensile tests. *J Mech Behav Biomed Mater* 53:257–271
- García-Herrera CM (2008) Mechanical behaviour of the human ascending aorta: characterization and numerical simulation. Ph.D. thesis (in Spanish), Universidad Politécnica de Madrid
- García-Herrera CM, Atienza JM, Rojo F, Claes E, Guinea GV, Celentano D, García-Montero C, Burgos R (2012a) Mechanical behaviour and rupture of normal and pathological human ascending aortic wall. *Med Biol Eng Comput* 50(6):559–566
- García-Herrera CM, Celentano DJ, Cruchaga MA, Rojo FJ, Atienza JM, Guinea GV, Goicolea JM (2012b) Mechanical characterisation of the human thoracic descending aorta: experiments and modelling. *Comput Methods Biomech Biomed Eng* 15:185–193
- García-Herrera CM, Celentano DJ (2013) Modelling and numerical simulation of the human aortic arch under in vivo conditions. *Biomech Model Mechanobiol* 12:1143–1154
- Grande-Allen KJ, Cochran RP, Reinhall PG, Kunzelman KS (2001) Mechanisms of aortic valve incompetence: finite-element modeling of Marfan syndrome. *J Thorac Cardiovasc Surg* 122(5):946–954
- Iliopoulos D, Deveja RP, Kritharis EP, Perrea D, Sionis GD, Toutouzias K, Stefanadis C, Sokolis D (2009) Regional and directional variations in the mechanical properties of ascending thoracic aortic aneurysms. *Med Eng Phys* 31:1–9
- Koullias G, Modak R, Tranquilli M (2005) Mechanical deterioration underlies malignant behavior of aneurysmal human ascending aorta. *J Thorac Cardiovasc Surg* 130:677.e1–677.e9
- Laurent S, Cockcroft J, Bortel LV, Boutouyrie P, Giannattasio C, Hayoz D, Pannier B, Vlachopoulos C, Wilkinson I, Struijker-Boudier H (2006) Expert consensus document on arterial stiffness: methodological issues and clinical applications. *Eur Heart J* 27:2588–2605
- Li Z, Kleinstreuer C (2005) A new wall stress equation for aneurysm-rupture prediction. *Ann Biomed Eng* 33:209–213
- Martufi G, Gasser TC, Appoo JJ, Di Martino ES (2014) Mechano-biology in the thoracic aortic aneurysm: a review and case study. *Biomech Model Mechanobiol* 13:917–928
- Medina E, Kaempffer A (2007) Enfermedades Cardiovasculares en Chile: Aspectos Epidemiológicos. *Rev Chil Cardiol* 26:219–226
- Meijboom L, Vos F, Timmermans J, Boers G, Zwinderman A, Mulder B (2005) Pregnancy and aortic root growth in the Marfan syndrome: a prospective study. *Eur Heart J* 26:914–920
- Merodio J, Haughton D (2010) Bifurcation of thick-walled cylindrical shells and the mechanical response of arterial tissue affected by Marfan's syndrome. *Mech Res Commun* 38:1–6

27. Nakagiri K, Kadowaki T, Morimoto N, Murakami H, Yoshida M, Mukohara N (2012) Aortic root reimplantation for isolated sinus of Valsalva aneurysm in the patient with Marfan's syndrome. *Ann Thorac Surg* 93:E49–E51
28. Nathan DP (2011) Pathogenesis of acute aortic dissection: a finite element stress analysis. *Ann Thorac Surg* 91:458–463
29. Nichols W, Rourke MO (1990) McDonald's flow in arteries theoretical, experimental and clinical principles, 3rd edn. Oxford University, New York
30. Nollen GJ, Groenink M, Tijssen JGP, van der Wall EE, Mulder BJM (2004) Aortic stiffness and diameter predict progressive aortic dilatation in patients with Marfan syndrome. *Eur Heart J* 25:1146–1152
31. Okamoto RJ, Wagenseil JE, DeLong WR, Peterson SJ, Kouchoukos NT, Sundt TM III (2002) Mechanical properties of dilated human ascending aorta. *Ann Biomed Eng* 30:624–635
32. Pape LA, Tsai TT, Isselbacher EM, Oh JK, O'gara PT, Evangelista A, Fattori R, Meinhardt G, Trimarchi S, Bossone E, Suzuki T, Cooper JV, Froehlich JB, Nienaber CA, Eagle KA (2007) Aortic diameter \geq 5.5 cm is not a good predictor of type aortic dissection. Observations from the International Registry of Acute Aortic Dissection (IRAD). *Circulation* 116(10):1120–1127
33. Pasta S, Phillippi JA, Gleason TG, Vorp DA (2012) Effect of aneurysm on the mechanical dissection properties of the human ascending thoracic aorta. *J Thorac Cardiovasc Surg* 143:460–467
34. Pasta S, Rinaudo A, Luca A, Pilato M, Scardulla C, Gleason TG, Vorp DA (2013) Difference in hemodynamic and wall stress of ascending thoracic aortic aneurysms with bicuspid and tricuspid aortic valve. *J Biomech* 46:1729–1738
35. Phillippi JA, Pasta S, Vorp DA (2011) Biomechanics and pathobiology of aortic aneurysms. *Stud Mechanobiol Tissue Eng Biomater* 7:67–118
36. Pichamuthu JE, Phillippi JA, Cleary DA, Chew DW, Hempel J, Vorp DA, Gleason TG (2013) Differential tensile strength and collagen composition in ascending aortic aneurysms by aortic valve phenotype. *Ann Thorac Surg* 96(6):2147–2154
37. Pruzinsky MS, Katz NM, Green CE, Satler LF (1988) Isolated descending thoracic aortic aneurysm in Marfan's syndrome. *Am J Cardiol* 61:1159–1160
38. Putz R, Pabst R, Weiglein A (2001) Sobotta atlas of human anatomic atlas, vol 2. Lippincott Williams & Wilkins, Philadelphia
39. Rose JL, Lalande A, Bouchot O, Bourennane EB, Walker PM, Ugolini P, Revol-Muller C, Cartier R, Brunotte F (2010) Influence of age and sex on aortic distensibility assessed by MRI in healthy subjects. *Magn Reson Imaging* 28:255–263
40. Vande Geest JP, Schmidt DE, Sacks MS, Vorp DA (2008) The effects of anisotropy on the stress analyses of patient-specific abdominal aortic aneurysms. *Ann Biomed Eng* 36:921–932
41. Vorp DA (2007) Biomechanics of abdominal aortic aneurysm. *J Biomech* 40:1887–1902
42. Vorp DA, Vande Geest JP (2005) Biomechanical determinants of abdominal aortic aneurysm rupture. *Arterioscler Thromb Vasc Biol* 25:1558–1566



Claudio M. García-Herrera is an Associate Professor in the Mechanical Engineering Department at Universidad de Santiago de Chile (USACH). His areas of research include Cardiovascular Biomechanics, Computational Mechanics and Solid Mechanics.



Diego J. Celentano is a Full Professor in the Mechanical and Metallurgical Department and Institute of Biological and Medical Engineering at Pontificia Universidad Católica de Chile (PUC). His areas of research include Computational Mechanics, Constitutive Models and Forming processes simulation.



Emilio A. Herrera is an Associate Professor and Director of Vascular Function and Reactivity Lab, Program of Pathophysiology, ICBM, Faculty of Medicine at Universidad de Chile (UCHILE). His areas of research include Vascular Reactivity, Cardiopulmonary Pathophysiology and hypoxia and oxidative stress.